*Progress In Electromagnetics Research M, Vol. 61, 61–73, 2017*

# Design of Double-Sided Linear Permanent Magnet Eddy Current Braking System

**Qiang Chen[1, *], Ying Tan[2], Guanchun Li[1], Jie Li[1], and Iven Mareels[2]**

**Abstract**—This work tries to design an Eddy current braking system that can brake at a very high speed within a short time or a short distance. In order to maximize the braking force and reduce lateral forces that can cause track deformation or damage, a double-sided linear permanent magnet Halbach array is proposed in this paper. Two possible designs (Type I and Type II) have been investigated. By using mathematic models, Finite Element Method (FEM) and experimental results, Type I design of a double-sided linear permanent magnet Halbach array is selected. Compared with the other design, Type I design can provide a much larger braking force. Moreover, the analysis also shows that the mathematic models can well capture the characteristic of Type I design. Thus these models are used to design a set of optimal design parameters such as the length and thickness of permanent magnet block to maximize flux density and braking force per unit mass of permanent magnets. The optimal performance is validated by using FEM.

## 1. INTRODUCTION

In some applications, braking systems need to handle very high speed within a short response time or a short distance. Examples include some high speed testing facilities used to ensure that the designed system can work safely, for example, the AFRL/RHPA Vertical Deceleration Tower (VDT) facility [1], as shown in Figure 1. Hydraulic friction braking systems [2] are usually used to provide enough frictions to decelerate quickly. Such a friction-based braking system is usually sensitive to conditions of contact surfaces. Furthermore, it always has a limited capacity in generating frictions. Besides, water and sand can be used to brake high speed ground testing systems [3]. Frictions are used to generate braking forces in these braking systems by having some physical contact with high speed moving vehicles. Due to the existence of such a physical contact, a large amount of friction forces are needed, leading to serious wear of the braking system with a high maintenance cost.

Eddy Current Braking (ECB) system [4] is a kind of non-contact braking method. It usually has a lower maintenance cost and longer service life. It is also less sensitive to various weather conditions. Hence it is more reliable when the safety is a major consideration in the design. Moreover, it can generate high braking forces at high speeds. Last but not least, it is environmentally friendly without dust or noises. Due to these advantages, the ECB system has been widely used in Maglev trains [5], electromagnetic launch systems [6], etc.

There are three different ways to generate magnetic forces for the ECB system. Compared with electromagnets and superconducting magnets, permanent magnets [7], which can maintain a constant magnetism after being magnetized, have the simplest structure as they need neither external power systems as needed in electromagnet systems nor complicated systems to maintain a low temperature as needed in superconducting magnets. Moreover, when a large braking force is needed, permanent

*Received 18 July 2017, Accepted 14 September 2017, Scheduled 12 October 2017*

* Corresponding author: Qiang Chen (Chen_NUDT@outlook.com).

[1] College of Mechatronics Engineering and Automation, National University of Defense Technology, Changsha 410073, China. [2] Department of Electrical and Electronic Engineering, The University of Melbourne, Parkville, VIC 3010, Australia.

**Figure 1.** AFRL/RHPA VDT facility.

magnets do not generate heating radiation caused by high current. However, the major disadvantages of permanent magnets is that once they are designed with fixed parameters, their characteristics will be fixed, making it impossible to adjust the performance. Therefore, the design of permanent magnets is crucial. Optimal performance is always needed.

As a special form of permanent magnet array, the Halbach array [8] can strengthen the magnetic field on one side of the permanent magnets while weaken the magnetic field on the other side through a special arrangement of the permanent magnets. Thus it can not only improve the magnetic field utilization, but also shield magnetic field effectively. Thus it can avoid strong magnetic field impact on other electronic equipment or human body. Characteristic and application of a single-sided ECB system with permanent magnetic Halbach array have been discussed [9–11].

In this paper, without the traditional friction-based braking method, an ECB system will be designed to a system like VDT facility, which has to brake a vehicle driving vertically at very high speed in a relative short distance. This system can be served as the testbed to check the effectiveness of ejection systems at high speed. In such a system, testing equipments is fixed on the carrier, which can move along the track. The carrier moves down from the top of the tower and stops at a certain height from the ground. The design requirements of the braking system can be summarized as follows:

(i) The braking demand is fixed, i.e., the speed should be reduced to the desired value within a given distance.

(ii) Safety plays an important role. Thus the design should avoid producing unnecessary forces, magnetic fields, temperature rise and other performances that will possibly cause damage of the ejection testing facility.

(iii) The part of the braking system mounted on the moving carrier is as light as possible to ensure the effective payload of the carrier.

The design of permanent magnet Halbach based ECB system can be found in Figure 2(a) and Figure 2(b). It usually consists of two parts. The primary part is the permanent magnet Halbach array mounted on the carrier. It moves with the carrier. The secondary part is a metal induction plate or induction coils fixed in the braking section of the tower. The primary is usually set on one side of the secondary. However, a single-sided linear ECB system will produce lateral force [10] ($y$-direction) perpendicular to the movement direction in addition to the braking force along the movement direction ($x$-direction). This lateral force is usually very large. Sometimes, it can be even larger than the braking force at a high speed. The presence of the lateral force may affect the performance of the test equipment. For the systems moving along the track, large lateral forces may cause track deformation or other damages. For example, in the application of a Maglev train, a large lateral force would affect the suspension or guidance system. If permanent magnet can be put on both sides of the secondary, as shown in Figure 2(c), it could offset the lateral force and enhance the magnetic field between two Halbach arrays to increase the braking force. To the best of the authors' knowledge, such a design does

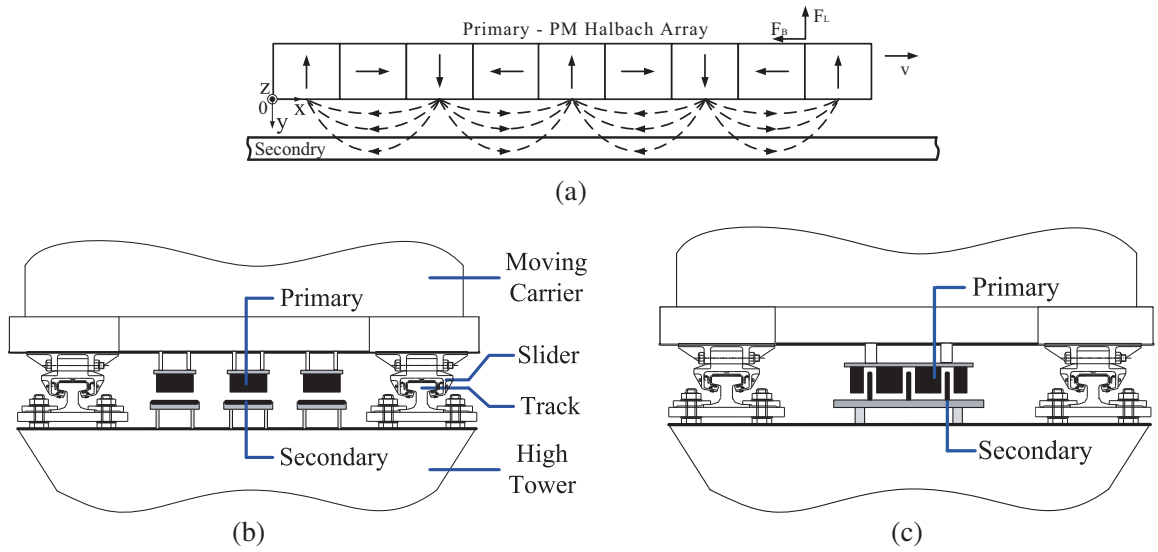


**Figure 2.** Ejection test facility with ECB systems. (a) Schematic diagram of a single-sided ECB system. (b) Top view of single-sided ECB. (c) Top view of double-sided ECB.

not exist in literature. Obviously, the design of a two-sided linear ECB is not unique, and how to choose a better design? If a particular design is selected, how to select the design parameters to achieve an optimal performance?

This paper tries to focus on answering above questions. A new two-sided linear ECB is designed. In order to obtain balanced performances including a strong braking force, no lateral force and good payload efficiency, this paper presents some design strategies with an optimal parameter selection to generate maximum flux density and braking force per unit mass of permanent magnets.

This paper is organized as follows. Section 3 compares two different types of double-sided design and selects one of them for our application. The model of magnetic field and electromagnetic forces are built and verified by FEM [12, 13], which is a standard numerical method for solving problems of engineering and mathematical physics. An experimental platform is built to verify the analysis. Section 3 optimally designs the double-sided linear permanent magnet ECB system. Section 4 summarizes the paper.

## 2. DESIGN OF DOUBLE-SIDED PERMANENT MAGNET HALBACH ARRAY

Two kinds of double-sided permanent magnet Halbach arrays, Type I and Type II, can be designed for the ECB system, as shown in Figure 3. The parameters used in the model are shown in Table 1.

### 2.1. Magnetic Field Analysis and Comparison between Type I and Type II

Shown in Figure 2(a), if the edge effects in the longitudinal direction ($x$ direction) and transverse direction ($z$ direction) are ignored [14], tt can be simplified as a 2D problem. The magnetic field distribution of a single-sided linear permanent magnet Halbach array in the gap can be described as follows:

$$B_x = B_0 \sin\left(kx + \frac{3\pi}{4}\right) e^{-ky}, \tag{1}$$

$$B_y = B_0 \cos\left(kx - \frac{\pi}{4}\right) e^{-ky}, \tag{2}$$

$$k = \frac{2\pi}{\lambda}, \tag{3}$$

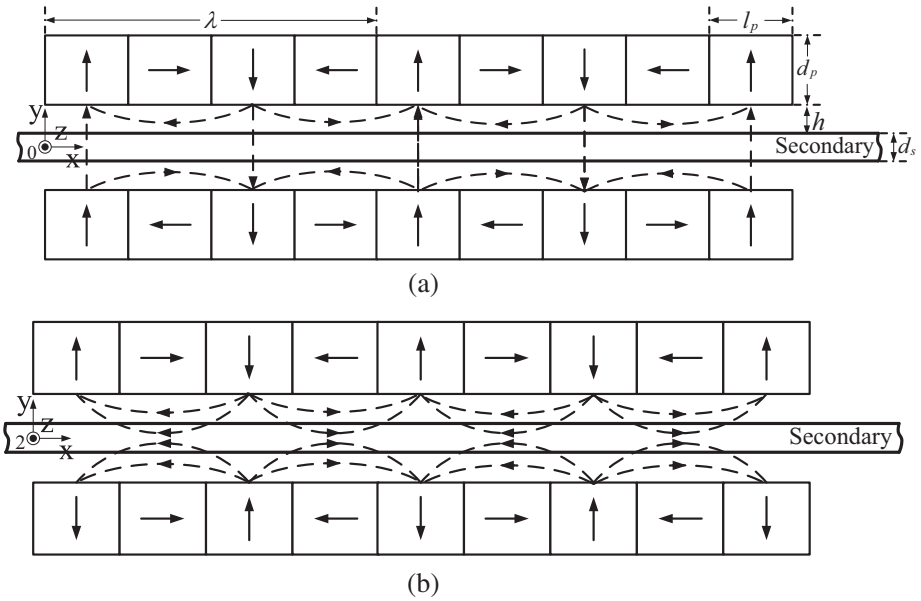


(a)

(b)

**Figure 3.** Schematic diagram of two kinds of Halbach arrays with magnetic field distribution. (a) Type I. (b) Type II.

**Table 1.** Parameters of the double-sided linear permanent magnet ECB system.

| | Parameters | Description | Value | Unit |
|---|---|---|---|---|
| Permanent Magnet | $l_p$ | Length | 30 | mm |
| | $d_p$ | Thickness | 25 | mm |
| | $w_p$ | Width | 50 | mm |
| | $B_r$ | Remanence | 1.33 | T |
| | $H_c$ | Coercivity | 796 | kA/m |
| Halbach Array | $\lambda$ | wavelength | 120 | mm |
| | $M$ | Permanent magnets number per wavelength | 4 | |
| | $p$ | Number of wavelengths | 2 | |
| Gap | $h$ | Gap between Halbach array and secondary | 10 | mm |
| Secondary (Aluminum Alloy) | $l_s$ | Length | 500 | mm |
| | $d_s$ | Thickness | 8 | mm |
| | $w_s$ | Width | 70 | mm |
| | $\sigma$ | Conductivity | $2.1 \times 10^7$ | s/m |

where $\lambda$ is the wavelength of Halbach array. $B_0$ is the flux density peak value of the magnetic field enhancement side of the permanent magnet Halbach array [15], and it can be computed as

$$B_0 = B_r \left[ \frac{\sin(\pi/M)}{\pi/M} \left(1 - e^{-kd_p}\right) \right], \tag{4}$$

where $B_r$ is the remanence of permanent magnet material, $M$ the permanent magnet block number of single wavelength Halbach array, and $d_p$ the thickness of permanent magnet block. The notion $d_s$ is the thickness of secondary, and $h$ is the gap between permanent magnetic Halbach array and secondary.

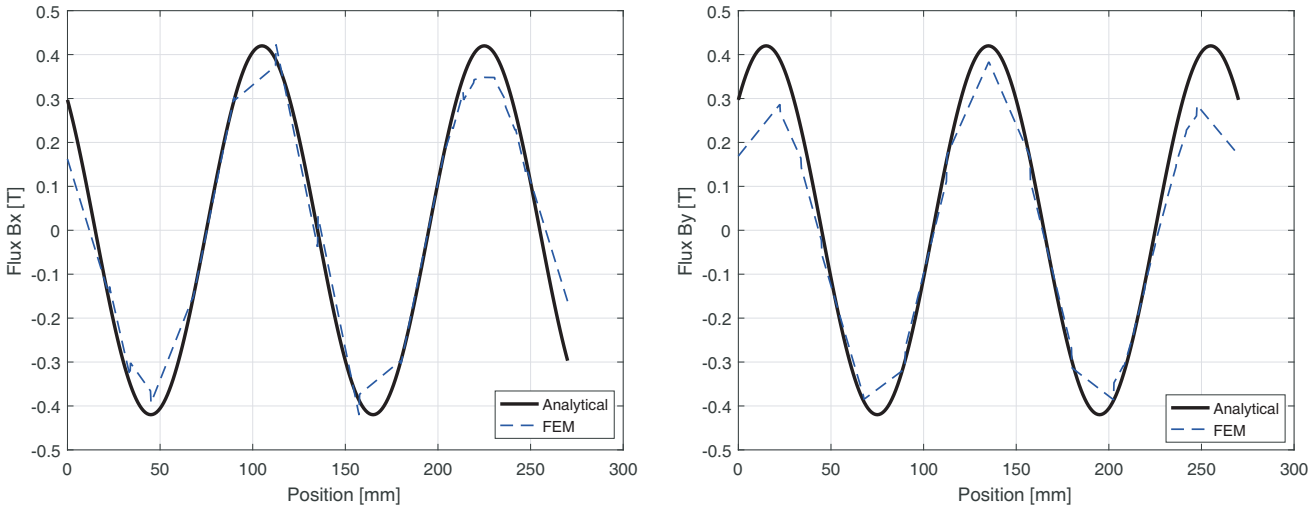


**Figure 4.** Magnetic field at 14 mm below the single-sided Halbach array. (a) $x$-direction component. (b) $y$-direction component.

Figure 4 shows the $x$-direction component and $y$-direction component of magnetic field at 14 mm below the single-sided Halbach array from theoretical analysis and FEM. It shows that the $x$-direction and $y$-direction components are both approximate sinusoidal distribution. Theoretical analysis results are slightly larger than the FEM results, especially at the end of the array, mainly caused by the edge effect.

As shown in Figure 3(a), magnetic field distribution in the gap can be represented as

$$\begin{aligned} B_{1x} &= B_{1xu} - B_{1xl} = B_0 \sin\left(kx + \frac{3\pi}{4}\right) e^{-k\left(\frac{1}{2}d_s+h\right)} \left(e^{ky} - e^{-ky}\right) \\ &= 2B_0 \sin\left(kx + \frac{3\pi}{4}\right) e^{-k\left(\frac{1}{2}d_s+h\right)} \sinh(ky) := \widetilde{B}_{1x} \sin\left(kx + \frac{3\pi}{4}\right), \end{aligned} \tag{5}$$

$$\begin{aligned} B_{1y} &= B_{1yu} + B_{1yl} = B_0 \cos\left(kx - \frac{\pi}{4}\right) e^{-k\left(\frac{1}{2}d_s+h\right)} \left(e^{ky} + e^{-ky}\right) \\ &= 2B_0 \cos\left(kx - \frac{\pi}{4}\right) e^{-k\left(\frac{1}{2}d_s+h\right)} \cosh(ky) := \widetilde{B}_{1y} \cos\left(kx - \frac{\pi}{4}\right), \end{aligned} \tag{6}$$

where $B_{1xu}$, $B_{1xl}$, $B_{1yu}$, $B_{1yu}$ are magnetic field of the upper and lower arrays in $x$-direction and $y$-direction, respectively.

Magnetic field distribution of Type I obtained from FEM is shown in Figure 5(a). Figure 5(b) and Figure 5(c) compare the $x$-direction and $y$-direction components of magnetic field in the middle of the two Halbach arrays between theoretical analysis and FEM. It is shown that the $x$-direction component of magnetic field is weakened and close to 0. The $y$-direction component is strengthened, and theoretical analysis results are slightly larger than the FEM ones.

Similarly, as shown in Figure 3(b), magnetic field distribution in the gap is:

$$B_{2x} = 2B_0 \sin\left(kx + \frac{3\pi}{4}\right) e^{-k\left(\frac{1}{2}d_s+h\right)} \cosh(ky) := \widetilde{B}_{2x} \sin\left(kx + \frac{3\pi}{4}\right), \tag{7}$$

$$B_{2y} = 2B_0 \cos\left(kx - \frac{\pi}{4}\right) e^{-k\left(\frac{1}{2}d_s+h\right)} \sinh(ky) := \widetilde{B}_{2y} \cos\left(kx - \frac{\pi}{4}\right). \tag{8}$$

The magnetic field distribution of Type II obtained from FEM is presented in Figure 6(a). Figure 6(b) and Figure 6(c) also compare the $x$-direction and $y$-direction components of magnetic field in the middle of the two Halbach arrays between theoretical analysis and FEM. It is shown that the $y$-direction component of magnetic field is weakened and close to 0. The $x$-direction component is strengthened, and theoretical analysis results are slightly larger than the FEM ones.

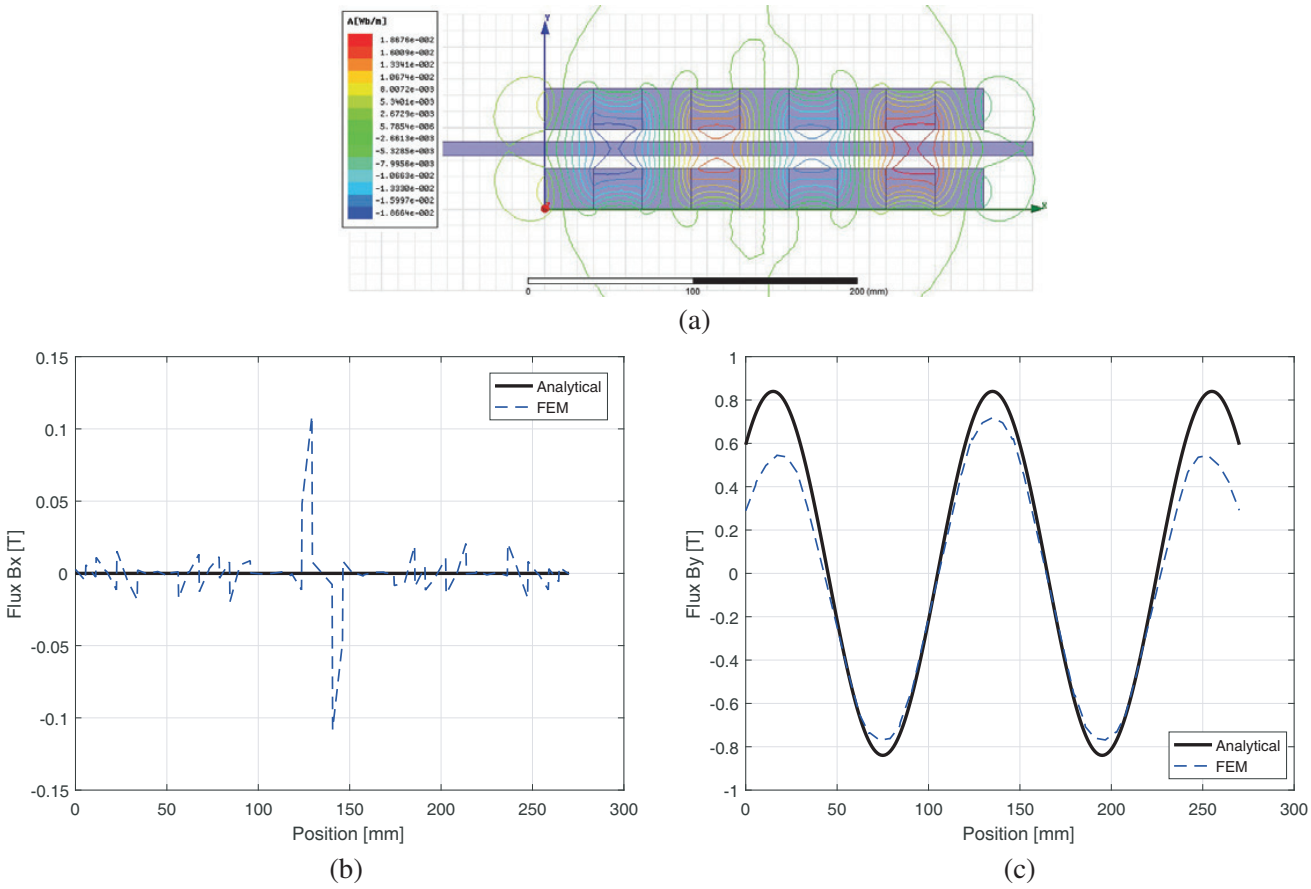


**Figure 5.** Magnetic field of the Type I. (a) Magnetic field obtained from FEM. (b) $x$-direction component. (c) $y$-direction component.

### 2.2. Braking Force Comparison and Analysis

The braking force $F_B$ and lateral force $F_L$ of permanent magnet Halbach array can be described as [16]:

$$F_B = C\widetilde{B}_y^2 \frac{\alpha}{1+\alpha^2}, \tag{9}$$

$$F_L = C\widetilde{B}_x\widetilde{B}_y \frac{1}{1+\alpha^2}, \tag{10}$$

where $\widetilde{B}_x$ and $\widetilde{B}_y$ represent the $x$-direction and $y$-direction components of the synthetic magnetic field of double-sided Halbach array, respectively. Constant $C$ is associated with the geometrical parameters of double-sided permanent magnet Halbach array and the secondary. Parameter $\alpha$ is computed as

$$\alpha = \frac{R}{L}\frac{1}{kv}, \tag{11}$$

where $R$ and $L$ represent the equivalent resistance and inductance of the unit wavelength secondary [17], and $v$ is the velocity of the permanent magnetic Halbach array which moves along the track.

From Equation (9), it can be seen that the braking force is related to the magnetic field strength in the $y$-direction, while $y$-direction component of magnetic field is strengthened in Type I whose transient magnetic field is shown in Figure 7(a), and it is weakened in type II whose transient magnetic field is shown in Figure 7(b). In order to compare the performance of two different designs, a ratio $\beta$ is used, i.e., $\beta$ is the ratio of the braking force $F_{1B}$ produced by Type I to the braking force $F_{2B}$ produced by

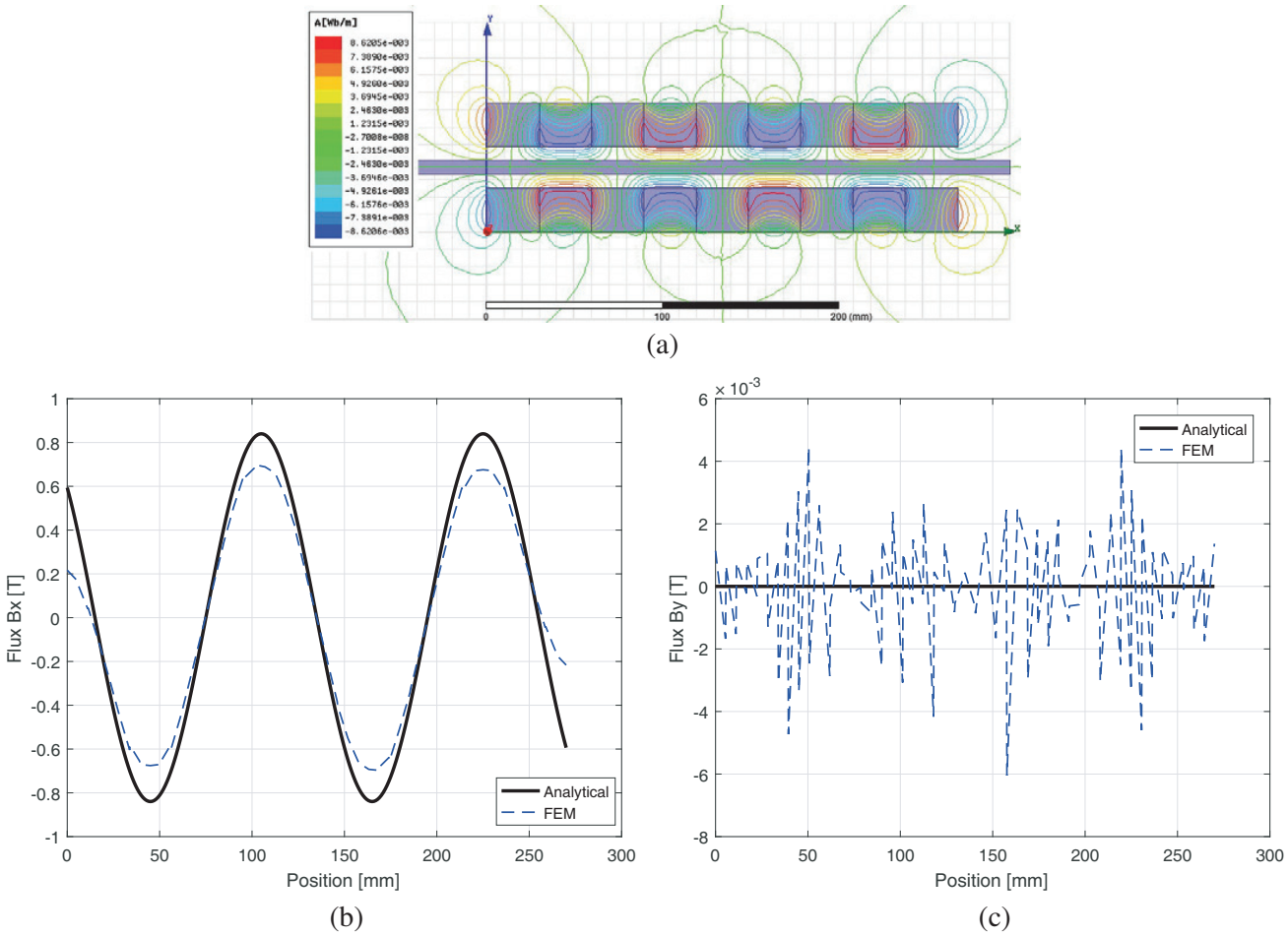


**Figure 6.** Magnetic field in the middle of the Type II. (a) Magnetic field obtained from FEM. (b) $x$-direction component. (c) $y$-direction component.

Type II.

$$\beta = \frac{F_{1B}}{F_{2B}} = \frac{\widetilde{B}_{1y}^2}{\widetilde{B}_{2y}^2} = \left[\frac{\cosh(ky)}{\sinh(ky)}\right]^2 = \coth^2(ky) > 1. \tag{12}$$

Figure 7(c) shows the braking force of Type I and Type II computed from FEM. This graph shows that $F_{1B}$ is always bigger than $F_{2B}$.

It can be seen clearly that $F_{2B}$ is very small and close to zero. Thus braking force $F_{1B}$ produced by Type I is much larger than $F_{2B}$ produced by Type II. With consideration of the largest possible braking force, the Type I design is suitable for an ECB system, while Type II could be used for a permanent magnet electrodynamic suspension system with a high levitation-to-drag ratio [18].

Under such a design, when braking, the permanent magnets move away from the conductive secondary part. It will generate induction and Eddy current in the secondary part. Consequently, the electromagnetic force is produced, which is in the opposite direction of the movement. In other words, the braking force is produced. This design will not only offset the lateral force by the double-sided setting, but also provide extra braking force by changing the distribution of the magnetic field.

### 2.3. Experimental Verification

By using the parameters in Table 1, a small scale ground experimental platform is designed and built, as shown in Figure 8. The experimental platform consists of a pneumatic catapult, a Type I double-

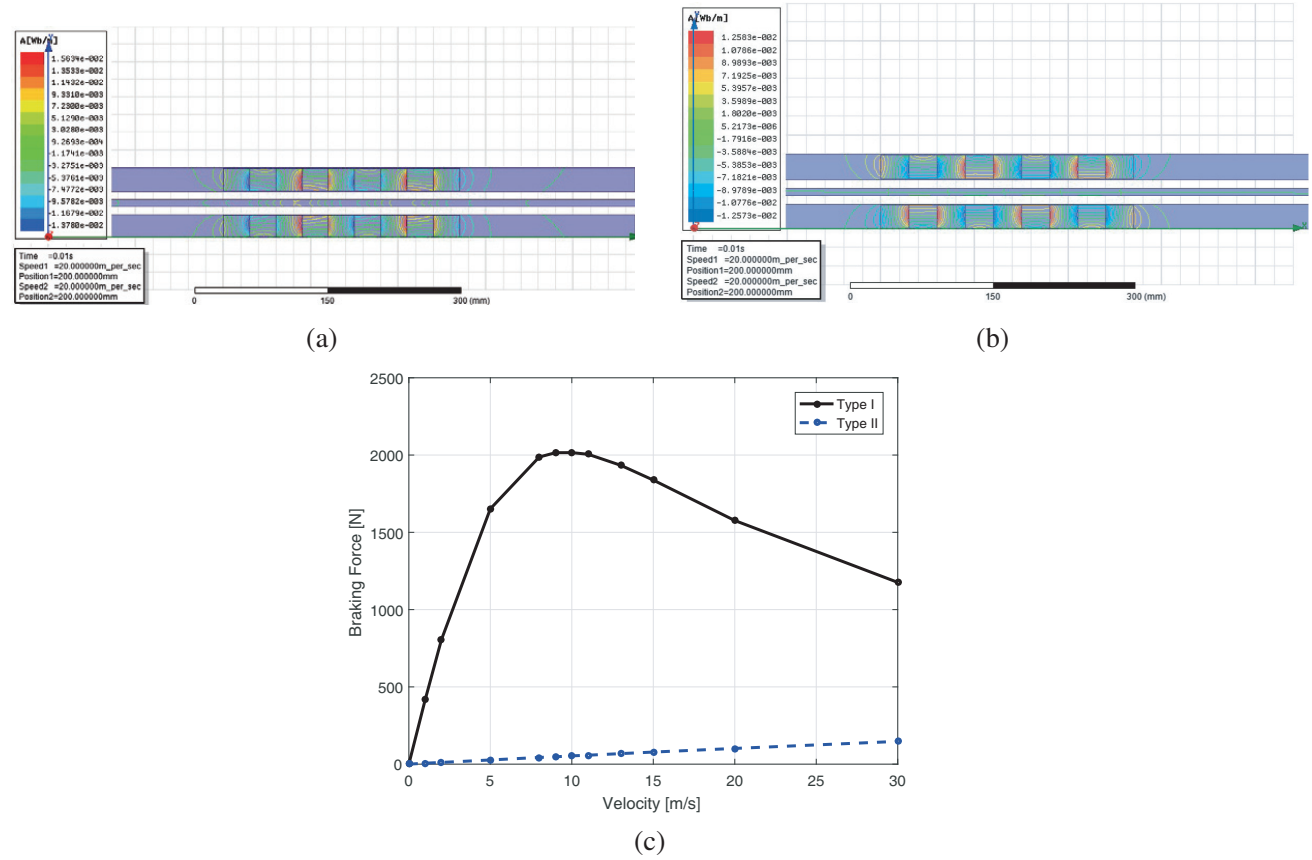


**Figure 7.** Dynamic behavior computed from FEM. (a) Transient magnetic field of Type I. (b) Transient magnetic field of Type II. (c) Braking force of Type I and Type II.

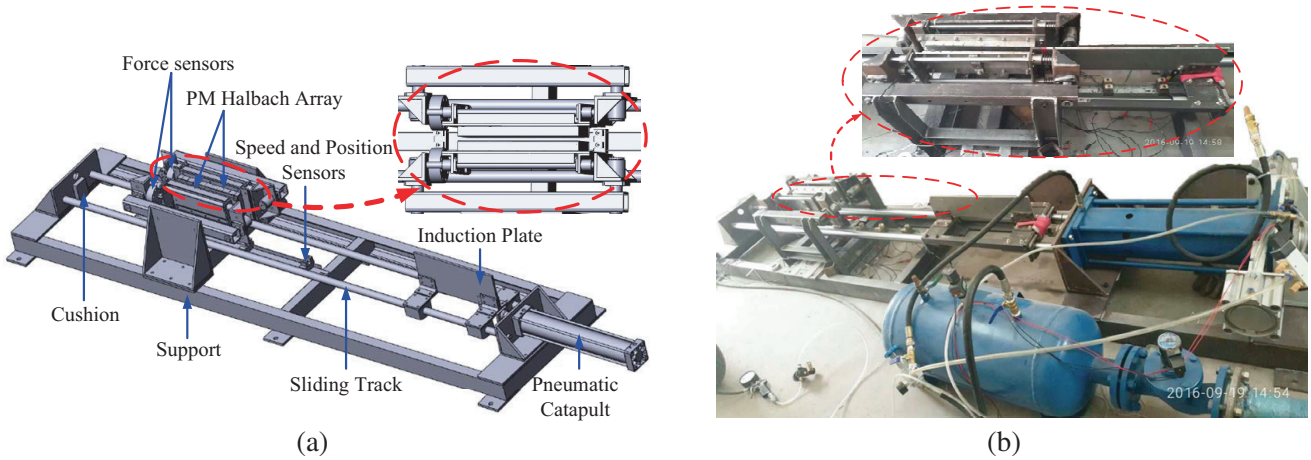


**Figure 8.** Double-sided linear permanent ECB experimental platform. (a) Schematic. (b) Photograph.

sided Halbach array, a secondary induction plate, velocity and position sensors, force sensors and a cushion. For the convenience of testing, the permanent magnet array is mounted on the support, and the secondary inductive plate is mounted on the moving carrier and moves along the sliding track.

Due to a small size and simple structure of the platform, the capacity of the experimental platform is limited, and the maximum ejection speed is about 20 m/s. Experimental, FEM, and theoretical results of braking force varying with different speeds are shown in Figure 9.

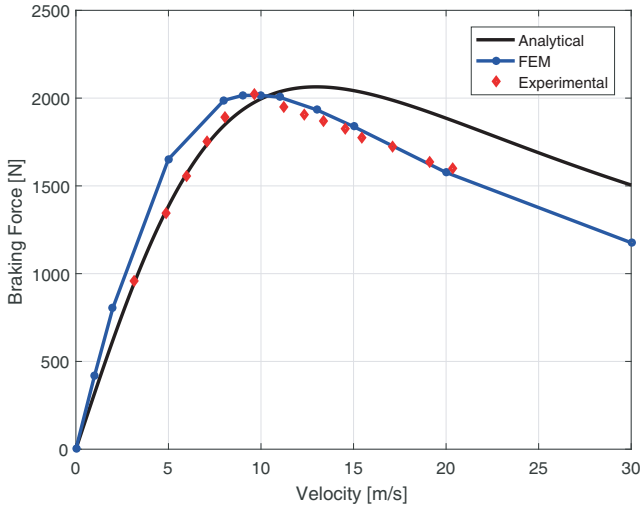


**Figure 9.** Experimental results, FEM results, and theoretical results of braking force varies with speed.

It can be seen that the speed corresponding to the maximum braking force from experiment and FEM is slightly lower than that of the theoretical results. When the speed is in a lower range, the braking force of FEM is slightly larger than that of theoretical analysis. When the speed is higher than the speed corresponding to the maximum braking force, braking force of FEM is slightly smaller than that of theoretical analysis. The maximum error of theoretical analysis from models and experimental results is about 16.78%. This verifies the theoretical analysis. Therefore, the models are suitable for performance analysis in terms of selecting optimal parameters. Moreover, the results from FEM are very consistent with the experimental ones. Thus, FEM can be used to validate the optimality of parameter sets.

## 3. OPTIMIZATION DESIGN

### 3.1. Characteristics Analysis of Braking Force

The characteristics of braking force can be obtained. Figure 10 shows that the curves of braking force vary with speed under the conditions of different gaps and conductivities of the secondary.

It can be seen that the smaller the gap is, the larger the braking force will be due to a larger magnetic field. Conductivity of the secondary part will not affect the maximum braking force much. However, they will affect the relationship between the braking force and the speed. Generally, if the secondary part has a better conductivity, it has a lower speed at the maximum braking force. Moreover, it will generate a larger braking force at a lower speed and a smaller braking force at a higher speed.

### 3.2. Geometric Structure Optimization Design of Permanent Magnet

The parameters of permanent magnets, secondary system and gap have influences on the braking force. However, for the permanent magnet ECB system, the permanent magnet array is generally mounted on the carrier and moves together. Therefore, in order to reduce the load and cost, it is necessary to optimize the design of permanent magnet structure [19]. Hence, an optimal design tries to use the least amount of permanent magnet material to obtain the maximum braking force by selecting optimal parameters.

As the size of the magnetic flux density of the permanent magnet Halbach array determines the size of the braking force, the optimization index can be selected as:

$$\gamma = \frac{\widetilde{B}_{1y}^2}{M_{PM}}, \tag{13}$$

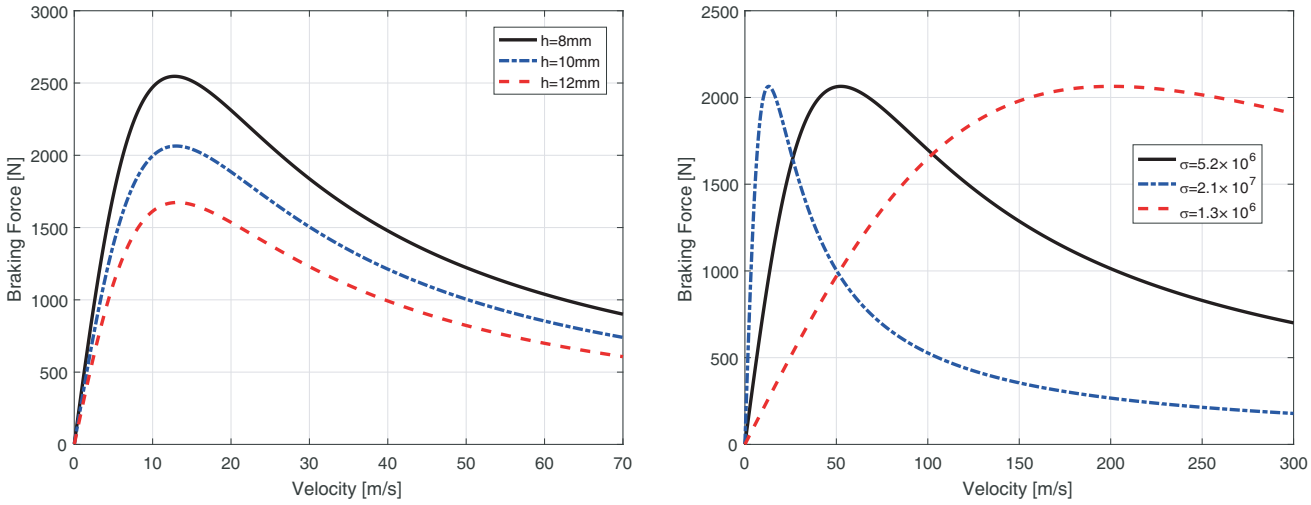


**Figure 10.** Braking force varies with speed under different conditions. (a) Different gap. (b) Different conductivity of secondary.

where $M_{PM}$ is the permanent magnets mass per unit area [20], which can be computed as:

$$M_{PM} = \rho d_p. \tag{14}$$

Here $\rho$ is the permanent magnet mass for per unit area and per unit thickness.

The objective of the optimization is to optimize the length ($l_p$) and thickness ($d_p$) of the permanent magnet so that the magnetic field generated by the permanent magnets per unit mass is the strongest, the maximum braking force obtained, and the utilization rate of the permanent magnets the highest.

In particular, on the surface of the secondary system, i.e., $y = \frac{1}{2}d_s$, it follows that

$$\widetilde{B}_{1y} = 2B_0 e^{-k\left(\frac{1}{2}d_s+h\right)} \cosh\left(\frac{1}{2}kd_s\right) = B_0 e^{-kh}\left(1+e^{-kd_s}\right). \tag{15}$$

This leads to

$$\begin{aligned}\gamma(k,d_p,d_s) &= \frac{B_0^2 e^{-2kh}\left(1+e^{-kd_s}\right)^2}{\rho d_p} \\ &= \frac{B_r^2}{\rho}\left[\frac{\sin(\pi/M)}{\pi/M}\right]^2 k e^{-2kh}\frac{\left(1-e^{-kd_p}\right)^2}{kd_p}\left(1+e^{-kd_s}\right)^2 \\ &= S_1 \cdot S_2(k) \cdot S_3(k,d_p) \cdot S_4(k,d_s).\end{aligned} \tag{16}$$

Here $S_1$ is defined as follows:

$$S_1 = \frac{B_r^2}{\rho}\left[\frac{\sin(\pi/M)}{\pi/M}\right]. \tag{17}$$

For a given Halbach array with a selected $M$, $S_1$ is a constant. Consequently, other functions in the index are:

$$S_2(k) = k e^{-2kh} \tag{18}$$

$$S_3(k,d_p) = S_3(\xi) = \frac{\left(1-e^{-\xi}\right)^2}{\xi} \tag{19}$$

$$\xi = kd_p \tag{20}$$

$$S_4(k,d_s) = \left(1+e^{-kd_s}\right)^2. \tag{21}$$

Note that for a fixed parameter $k$, the function $S_4(k, d_s) > 1$ monotonically decreases in terms of positive $d_s$. That is, a smaller thickness of the secondary will lead to a smaller distance between two Halbach arrays and a stronger magnetic field in the gap. There are physical constraints of $d_s$. When designing, the braking demand, mechanical structure space and strength should be considered. Besides, with the consideration of the skin effect [21], the thickness of the secondary should be slightly less than the skin depth to ensure that magnetic field can pass through the secondary. Assume that with the consideration of these physical constraints, the smallest possible $d_s$ is obtained.

Next, how to choose optimal $k$ and $d_p$ to maximize $\gamma$ will be shown in Eq. (16). Note that the function $S_3(\cdot)$ is only a function of $\xi$. In order to reach a maximum of $S_3(\xi)$ with respect to $\xi$, taking partial derivative of $S_3$ yields:

$$\frac{\partial S_3}{\partial \xi}(\xi) = 2(1+\xi)\left(e^{-\xi} - e^{-2\xi}\right) - 1. \tag{22}$$

At $\xi = \xi^*$, $\frac{\partial S_3}{\partial \xi}(\xi^*) = 0$. It indicates that at $\xi^* \approx 1.2564$, $S_3(\xi)$ reaches its maximum value. Therefore, $d_p^* \approx \frac{1.2564}{k}$.

Then the last one to handle in Eq. (16) is $S_2(k)$. Taking the partial derivative of $S_2(\cdot)$ with respect to $k$ becomes

$$\frac{\partial S_2}{\partial k}(k) = (1-2hk)e^{-2kh}, \tag{23}$$

thus $S_2(k)$ reaches its maximum at $k^* = \frac{1}{2h}$. This yields an optimal $d_p^* \approx 2.5128h$.

When designing, the gap $h$ is usually first selected according to braking demands. In a word, with a given appropriate gap $h$, material and thickness of the secondary system, in order to maximize $\gamma$, the structure of Halbach array should be selected according to the optimal geometric structure of permanent magnet computed as:

$$l_p^* = \frac{4}{M}\pi h \tag{24}$$

$$d_p^* \approx 2.5128h \tag{25}$$

Table 1 shows the optimal parameters designed according to the optimization index, respectively changing geometrical parameters of the permanent magnet to make $l_p = 40$, $l_p = 50$, $d_p = 35$, $d_p = 45$. Braking forces per unit mass of permanent magnets from FEM are shown in Figure 11.

It can be seen that the optimized parameters make the maximum braking force per unite mass, which means that in the same braking force demand, fewer permanent magnets are used. It not only increases the effective payload but also reduces the cost.

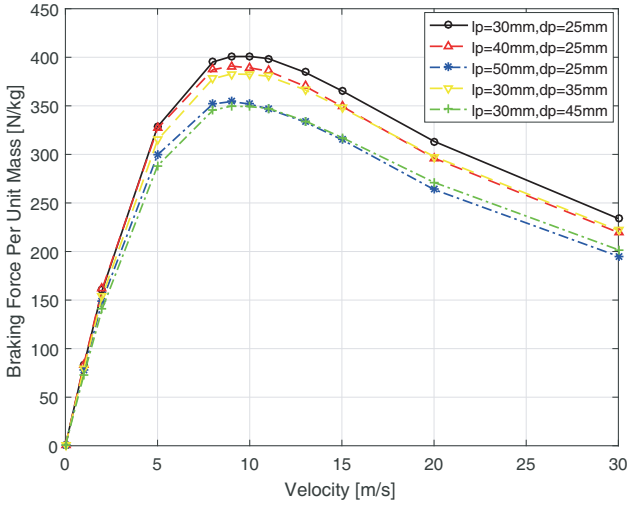


**Figure 11.** Braking force per unit mass of permanent magnets from different parameters.

## 4. CONCLUSION

For a facility like VDT, the ECB system is used in order to stop a vehicle driving vertically at very high speed. In order to produce a large braking force with almost zero lateral force, a double-sided permanent magnet Halbach array is selected. Using mathematical models, validated from FEM and experiments, a set of optimal structure parameters of permanent magnets are designed to obtain the best performance. The effectiveness of such an optimal design has been validated by a high speed testing facility.

## REFERENCES


1. Perry, C. E., "Vertical impact tests of a proposed B-52 ejection seat cushion," Human Effectiveness Directorate Wright-Patterson AFB OH 711 Human Performance Wing, 2007.
2. Brinkley, J. W., C. E. Perry, M. D. Salerno, et al., "Evaluation of a proposed F-4 ejection seat cushion by +Gz impact tests," Armstrons Lab Wright-Patterson AFB OH Crew Systems Directorte, 1993.
3. Turnbull, D., C. Hooser, M. Hooser, et al., "Soft sled test capability at the holloman high speed test track," US Air Force T&E Days 1708, 2010.
4. Yazdanpanah, R. and M. Mirsalim, "Analytical study of axial-flux hybrid excitation eddy current brakes," *International Journal of Applied Electromagnetics and Mechanics*, Vol. 47, No. 4, 885–896, 2015.
5. Thompson, M. T., "Practical issues in the use of NdFeB permanent magnets in maglev, motors, bearings, and eddy current brakes," *Proceedings of the IEEE*, Vol. 97, No. 11, 1758–1767, 2009.
6. Wu, J., Y. Yang, H. Zhao, et al., "Hybrid brake method for electromagnetic launcher of unmanned aerial vehicle," *Journal of National University of Defense Technology*, Vol. 5, 010, 2015.
7. Sagawa, M., S. Hirosawa, H. Yamamoto, et al., "NdFeB permanent magnet materials," *Japanese Journal of Applied Physics*, Vol. 26, No. 6R, 785, 1987.
8. Halbach, K., "Application of permanent magnets in accelerators and electron storage rings," *Journal of Applied Physics*, Vol. 57, No. 8, 3605–3608, 1985.
9. Jang, S. M., S. S. Jeong, and S. D. Cha, "The application of linear Halbach array to eddy current rail brake system," *IEEE Transactions on Magnetics*, Vol. 37, No. 4, 2627–2629, 2001.
10. Jang, S. M., S. H. Lee, and S. S. Jeong, "Characteristic analysis of eddy-current brake system using the linear Halbach array," *IEEE Transactions on Magnetics*, Vol. 38, No. 5, 2994–2996, 2002.
11. Wang, J. B., Y. H. Li, and L. G. Yan, "Study on applying the linear Halbach array to eddy current brake system," *International Journal of Applied Electromagnetics and Mechanics*, Vol. 33, No. 1, 2, 111–118, 2010.
12. Wang, H. and K. L. Butler, "Finite element analysis of internal winding faults in distribution transformers," *IEEE Transactions on Power Delivery*, Vol. 16, No. 3, 422–428, 2001.
13. Ansoft Corporation, Maxwell Software, Elmwood Park, Ansoft Corporation, NJ, 1998.
14. Post, R. F., "Inductrack demonstration model," Lawrence Livermore National Lab., CA (United States), 1998.
15. Post, R. F. and D. D. Ryutov, "The inductrack: A simpler approach to magnetic levitation," *IEEE Transactions on Applied Superconductivity*, Vol. 10, No. 1, 901–904, 2000.
16. Kratz, R. and R. F. Post, "A null-current electro-dynamic levitation system," *IEEE Transactions on Applied Superconductivity*, Vol. 12, No. 1, 930–932, 2002.
17. Post, R. F. and D. Ryutov, "The inductrack concept: A new approach to magnetic levitation," Lawrence Livermore National Lab., CA (United States), 1996.
18. Gurol, S., R. Baldi, D. Bever, et al., "Status of the general atomics low speed urban maglev technology development program," Lawrence Livermore National Laboratory (LLNL), Livermore, CA, 2004.
19. Davey, K., "Optimization shows Halbach arrays to be non-ideal for induction devices," *IEEE Transactions on Magnetics*, Vol. 36, No. 4, 1035–1038, 2000.

20. Han, Q., C. Ham, and R. Phillips, "Four-and eight-piece Halbach array analysis and geometry optimisation for maglev," *IEE Proceedings — Electric Power Applications*, Vol. 152, No. 3, 535–542, 2005.
21. Jafari-Shapoorabadi, R., A. Konrad, and A. N. Sinclair, "Comparison of three formulations for eddy-current and skin effect problems," *IEEE Transactions on Magnetics*, Vol. 38, No. 2, 617–620, 2002.